A Traveling-Wave High Electron Mobility Transistor

M. B. Anand, Prasanta K. Ghosh, *Senior Member, IEEE,* Philipp G. Kornreich, *Member, IEEE,* and D. J. Nicholson

***Abstract*— A traveling-wave high electron mobiligy transistor (THEMT) is proposed. The proposed device is unique in that it includes an integral distributed load resistor and that it uses a high electron mobility transistor as the active device. A rigorous analysis of the device is carried out, using a small-signal equivalent circuit model for an incremental secton of the device. Losses and reflected waves are not neglected, as has been done in other work. Treating the device as a 4-port network, closed-form expressions for S-parameters are derived, we believe for the first time. Theoretical calculations using equivalent circuit parameter values of a HEMT reported in the literature, show that the proposed device is capable of exponential increase in gain with device width. Power gain of more than 10 dB at 50 GHz and remarkably flat response in the frequency range 10 GHz to 100 GHz are shown to be achievable for a 1 mm wide device.**

I. Introduction

THE CONCEPT of integral traveling wave structures is not new. In these devices, a field effect transistor structure is stretched out along its width to take advantage of the increased signal transit time and thus obtain higher bandwidth and gain. McIver [1] proposed one such structure in which the gain of the device increases exponentially with the device width. McIver's simplified analysis was supplemented by W. Jutzi [2], Kohn and Landauer [3], who showed that passive reactance coupling between gate and drain lines provides for automatic phase velocity synchronism in the gate and drain lines, and thus exponential signal growth. Recently, several authors have addressed this topic [4]–[6]. Podgorski and Wei [4] proposed and analyzed two traveling-wave structures using Schottky-barrier field-effect transistors, but their analysis neglects coupling due to parasitics. Further, these structures are difficult to fabricate since they require multi-level technology. Ce-Jun Wei [5] and A. J. Holden *et al.* [6] have also considered traveling-wave field-effect structures.

We propose a traveling wave high electron mobility transistor (THEMT). The proposed device is different from all previous work in that it includes an integral distributed load resistor which is useful in controlling device response and it uses a high electron mobility transistor (HEMT) as the active element. Ce-Jun Wei's structure [5] is somewhat similar but he uses an image gate with an adjustable bias instead. We present a rigorous analysis of the proposed structure. A transistor equivalent circuit model for an incremental section of the device is used to derive solutions for the traveling waves in the structure. The transmission lines are treated as lossy structures. Reflected waves are not neglected in contrast to Ce-Jun Wei's work and passive reactance coupling due to parasitics is not neglected either, unlike Podgorski and Wei's work. In addition we derive, we believe for the first time, a complete S-parameter formulation of the device in closed form treating the device as a 4-port network. The S-parameter expressions are used to show the frequency response of the device and the variation of its gain with the device width. Equivalent circuit parameter values of a HEMT reported in the literature [7] are used in all these calculations. Further, we show that the presence of exponentially growing waves in the device is critically dependent on the equivalent circuit element values by demonstrating a case where the device actually produces an exponential attenuation instead of growth. In this context, the importance of the integral load resistor as means of "tuning" the device to produce the desired exponential growth, of the gain is shown.

Manuscript received March 28, 1990; revised July 15, 1992.

M. B. Anand, P. K. Ghosh and P. G. Kornreich are with the Department of Electrical and Computer Engineering, Syracuse University, Syracuse, NY 13244-1240.

D. J. Nicholson is with RADC/DCLW, Griffiss AFB, Rome, NY 13440.

IEEE Log Number 9206308.

II. Proposed Structure

The structure of the proposed device is shown in Fig. 1. The underlying transistor structure is the normal HEMT structure. The transmission line structure that supports traveling waves is fabricated on the top wide gap semiconductor layer as follows: a wide metal strip ohmically connected to the channel through a highly doped region forms the distributed source of the device. This strip is grounded since the device is operated in the common source configuration. Next to the source line is a metal strip which forms a Schottky barrier contact to the top wide gap semiconductor layer. This forms the distributed gate of the device. The electronically completely depleted top layer under the gate line forms the gate insulation. The next metal line, also ohmically connected to the channel forms the distributed drain of the device. The forth metal line, again ohmically connected to the channel, is the supply line. It is connected to a dc supply voltage and is an ac ground. The integral load resistor with its parallel load capacitance is made up of the portion of the channel between the supply and drain line.

III. Analysis

A. Dispersion Relation

The dispersion relation expresses the propagation constants of the modes present in the device as a function of the frequency. This expression is useful in deducing information about the nature of the modes, as shown later in this section; the signs of the real and imaginary parts of the propagation

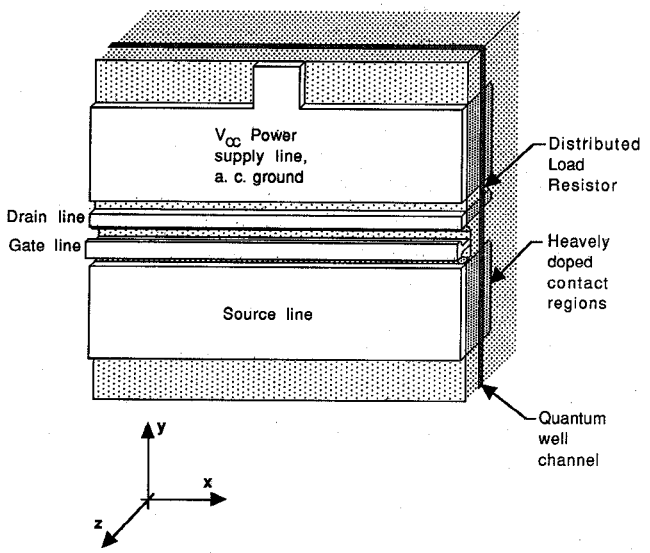

Fig. 1. Structure of the THEMT.

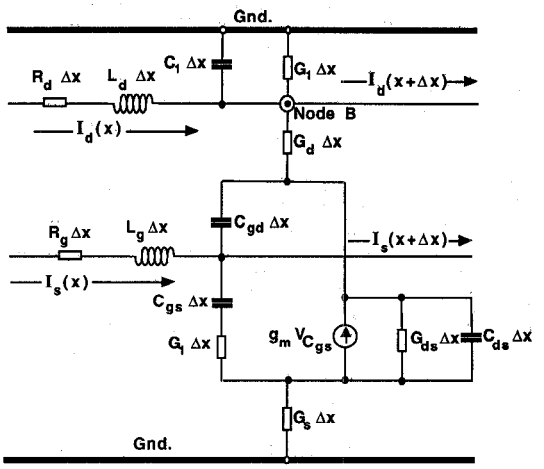

Fig. 2. Equivalent circuit of an incremental section of the THEMT.

constants help in deducing whether a mode is forward or reverse-traveling, growing or decaying.

The dimensions of the device in the y-z plane are much smaller than a wavelength at the maximum operating frequency considered, 100 GHz. This allows us to model the device by incremental lumped circuit parameters. The equivalent circuit of an incremental section of the device is shown in Fig. 2. This model, is due to [7] except for the load resistor G_1 and load capacitor C_1. Referring to Fig. 2, the loop equations for loops 1 and 2 are, respectively:

$$[V_g(\omega, x+\Delta x) - V_g(\omega, x)]/\Delta x = -(R_g + j\omega L_G) I_g(\omega, x) \quad (1)$$

$$[V_d(\omega, x+\Delta x) - V_d(\omega, x)]/\Delta x = -(R_d + j\omega L_d) I_d(\omega, x). \quad (2)$$

The nodal equations for nodes A and B in Fig. 2 are, respectively:

$$[I_g(\omega, x+\Delta x) - I_g(\omega, x)]/\Delta x = M_{11}(\omega)\, V_g(\omega, x+\Delta x) + M_{12}(\omega)\, V_d(\omega, x+\Delta x) \quad (3)$$

$$[I_d(\omega, x+\Delta x) - I_d(\omega, x)]/\Delta x = M_{21}(\omega)\, V_G(\omega, x+\Delta x) + M_{22}(\omega)\, V_d(\omega, x+\Delta x) \quad (4)$$

where $M_{ij}(\omega)$ are complex non-standard admittance parameters per unit width of the device and $I_i(\omega, x)$ and $V_j(\omega, x)$, are phasor voltages and currents. The derivation of the $M_{ij}(\omega)$ from a detailed loop and nodal analysis of the equivalent circuit is given in the Appendix.

In the limit as Δx goes to zero the differences in the above equations become differentials and we obtain the Telegrapher's equations relating gate voltage and current with those of the drain and through M parameters (Appendix). From those we obtain the following coupled second order differential equations for the voltages on the gate and drain:

$$d^2V_g/dx^2 + Z_g M_{11} V_g + Z_g M_{12} V_d = 0 \quad (5)$$

$$d^2V_d/dx^2 + Z_d M_{21} V_g + Z_d M_{22} V_d = 0. \quad (6)$$

Since a two-coupled transmission line system is being considered, two modes of propagation, each with forward and reverse traveling waves, must exist in this device. Thus, four exponential terms must be present in both the solutions for V_g and V_d. Accordingly, we assume the following traveling-wave solutions for the voltages in the above two simultaneous differential equations:

$$V_g = A_1 e^{\gamma_1 x} + A_2 e^{\gamma_2 x} + A_3 e^{-\gamma_1 x} + A_4 e^{-\gamma_2 x} \quad (7)$$

$$V_d = B_1 e^{\gamma_1 x} + B_2 e^{\gamma_2 x} + B_3 e^{-\gamma_1 x} + B_4 e^{-\gamma_2 x}. \quad (8)$$

An exactly similar procedure for the currents yields

$$I_g = C_1 e^{\gamma_1 x} + C_2 e^{\gamma_2 x} + C_3 e^{-\gamma_1 x} + C_4 e^{-\gamma_2 x} \quad (9)$$

$$I_d = D_1 e^{\gamma_1 x} + D_2 e^{\gamma_2 x} + D_3 e^{-\gamma_1 x} + D_4 e^{-\gamma_2 x}. \quad (10)$$

Where the A's, B's, C's and D's are constants which depend on the boundary conditions, γ_1 and γ_2 are the propagation constants of the two modes mentioned above and the $e^{\gamma x}$ and $e^{-\gamma x}$ terms indicate forward and reverse traveling waves. The solutions for γ_1 and γ_2 are obtained from the coupled wave equations (5) and (6) as:

$$\gamma_{1,2} = \{-(k_{11}+k_{22})/2 \pm [(k_{11}+k_{22})^{2/4} - (k_{11}k_{22} - k_{12}k_{21})]^{1/2}\}^{1/2} \quad (11)$$

where $k_{11} = Z_g M_{11}, k_{12} = Z_g M_{12}, k_{21} = Z_d M_{21}$ and $k_{22} = Z_d M_{22}$. The "1" and "2" subscripts of 8, 7 correspond to the "$\pm$ " in (11).

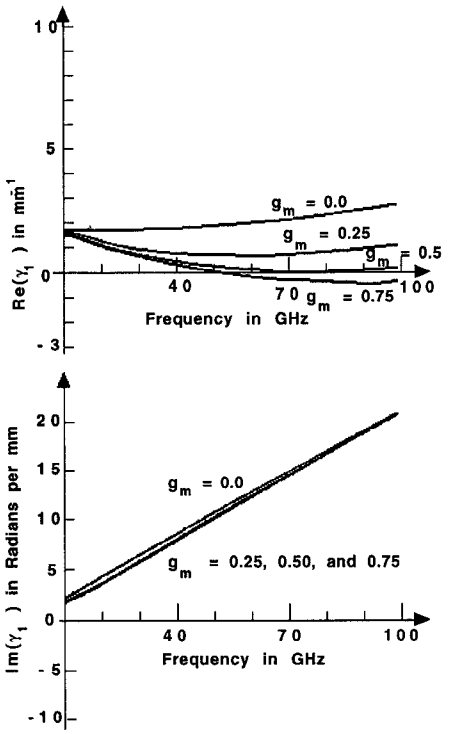

Fig. 3. Real and imaginary parts of γ_1 as a functions of frequency. Values of g_m are in S/mm.

Real and imaginary parts of γ_1 as functions of frequency are shown in Fig. 3; the equivalent circuit parameter values used in these plots are taken from reference [7] except for the following assumed values, $G_1 = 0.01$ S/mm and $C_1 = 0.48467$ pF/mm. These values are selected after several tests to demonstrate possible different nature of the resulting waves. The imaginary part is positive for all values of frequency and g_m; further, it is almost linear with frequency. This indicates that the phase velocity of this mode is almost completely independent of frequency. The real part is also positive for the most values of g_m but does however, become negative for frequencies above 50 GHz and for $g_m = 0.75$ S/mm. Our results indicate the combination of positive real and imaginary parts creates a decaying mode; whereas, the combination of negative real part and positive imaginary results in part a growing mode. Thus, for the set of equivalent circuit parameter values used, γ_1 is a decaying mode for frequencies less than 50 GHz, for all values of g_m considered, but turns into a growing mode for frequencies above 50 GHz at $g_m = 0.75$ S/mm. A plot of the real and imaginary parts of γ_2 (not shown) indicates that this mode is a decaying one for all values of g_m over the whole range of frequencies considered.

B. S-Parameters

To derive the S-parameter expressions, we begin by embedding the device in a transmission line structure, as shown in Fig. 4. The S-parameters obtained would then be normalized to the characteristic impedances of the feeder transmission lines at the respective ports. For the sake of simplicity, we assume the characteristic impedances of all four feeder transmission

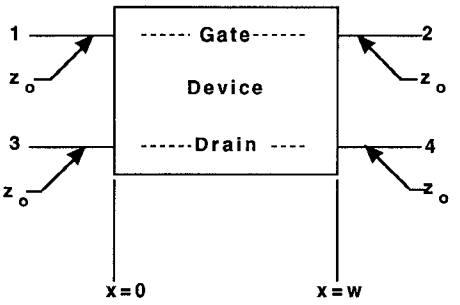

Fig. 4. Embedded structure used in S-parameter derivation.

lines to be equal to Z_0; this assumption will, however, be generalized later.

The number of unique, nonzero S-parameters and the form of the S-matrix can be obtained by applying the following arguments. Since ports 1 & 3 and 2 & 4 assumed to lie on exactly the same sectional planes of the device, the coupling between ports 1 & 3 and 2 & 4 must be equal to zero. This means that S_{13} and S_{31}, S_{24} and S_{42} should all be equal to zero. Further, the lateral symmetry of the device along its width dictates that ports 1 and 2 be interchangeable; similarly ports 3 and 4 are interchangeable. Using these arguments the S-matrix of the proposed device can be deduced to be of the form shown below in (12).

We first note that the sets of constants A_i, B_i, C_i and D_i $(i = 1, 2, 3, 4)$ in the (3) through (6) are not independent of each other. In fact since the voltages and currents are coupled by the circuit equations only one set of constants is needed to completely define the other three. Using (1) and substituting for V_g and V_d from the solutions (3) and (4), we obtain:

$$[S] = \begin{vmatrix} S_{11} & s_{12} & 0 & S_{14} \\ S_{12} & S_{11} & S_{14} & 0 \\ 0 & S_{32} & S_{33} & S_{34} \\ S_{32} & 0 & S_{34} & S_{33} \end{vmatrix} \tag{12}$$

$$B_1 = -(\gamma_1^2 + k_{11})A_1/k_{12} \tag{13a}$$

$$B_2 = -(\gamma_2^2 + k_{11})A_2/k_{12} \tag{13b}$$

$$B_3 = -(\gamma_1^2 + k_{11})A_3/k_{12} \tag{13c}$$

$$B_4 = -(\gamma_2^2 + k_{11})A_4/k_{12}. \tag{13d}$$

Using the Telegrapher's equation and substituting for V_g and I_g in it from solutions (3) and (5) respectively, we obtain expressions for the C's in terms of the A's and substituting for V_d and I_d in Telegrapher's equation from solutions (4) and (6) respectively, we obtain D's in terms of A's.

Thus all constants can be defined in terms of the A's.

The defining equation for the S-parameters is

$$[B] = [S][A]. \tag{14}$$

Where $[B]$ are the reflected "power" waves at all the ports and $[A]$ are the incident power waves. Since we have assumed that the normalization impedances are the same at all ports, the same S -matrix also relates incident and reflected voltage waves. Now, the voltage on the feeder transmissions lines of ports 1 and 3 can be expressed in terms of the boundary

voltage and current, in this case the load voltage and current, as follows [8]:

$$V = e^{\gamma x}(V_b + I_b Z_0)/2 + e^{-\gamma x}(V_b - I_b Z_0)/2 \tag{15}$$

where V_b and I_b are the boundary voltage and current respectively. " γ" in the above equation refers to the propagation constant in the feeder transmission line and is not to be confused with the propagation constants in the device itself. Referring to Fig. 4, port 1 corresponds to the $x = 0$ end of the gate line. Thus, putting $x = 0$ in the solutions for V_g and I_g, (3) and (5), we obtain:

$$V_{1b} = A_1 + A_2 + A_3 + A_4 \tag{16}$$

$$I_{1b} = C_1 + C_2 + C_3 + C_4 \tag{17}$$

In (15), we note that the $e^{\gamma x}$ terms corresponds to a wave traveling in the negative x direction, and the $e^{-\gamma x}$ term corresponds to a wave traveling in the positive x direction. Thus, the former constitutes the reflected wave and the latter the incident wave at port 1. Substituting eqns. (16) and (17) into (15) and making use of the relations between the C's and A's derived earlier, we can then write, for the reflected and incident waves at port 1,

$$\begin{aligned} V_1^- = {} & A_1 \frac{(Z_g + \gamma_1 Z_0)}{2Z_g} \\ & + A_2 \frac{(Z_g + \gamma_2 Z_0)}{2Z_g} \\ & + A_3 \frac{(Z_g - \gamma_1 Z_0)}{2Z_g} \\ & + \frac{(Z_g - \gamma_2 Z_0)}{2Z_g} \end{aligned} \tag{18}$$

or,

$$V_1^- \doteq mA_1 + nA_2 + oA_3 + pA_4 \tag{19}$$

and,

$$V_1^+ = oA_1 + pA_2 + mA_3 + nA_4 \tag{20}$$

where V_1^- stands for the reflected voltage wave, V_1^+ stands for the incident voltage wave. Note that the length of the feeder transmission line is assumed to be zero in (19) and (20). This is done to calculate the S-parameters of the device itself i.e., to avoid including the phase difference introduced by the transmission lines; it is however, a simple transformation of the S-matrix to include finite-length transmission lines, once the S-parameters of the device are calculated. For port 3, the boundary voltage and current are,

$$V_{3b} = B_1 + B_2 + B_3 + B_4 \tag{21}$$

$$I_{3b} = D_1 + D_2 + D_3 + D_4 \tag{22}$$

Substituting (21) and (22) into (15) and using (2) and (3) we obtain:

$$\begin{aligned} V_3^- = {} & -A_1 \frac{(Z_d + \gamma_1 Z_0)(\gamma_1^2 + k^{11})}{2k_{12} Z_d} \\ & - A_2 \frac{(Z_d + \gamma_2 Z_0)(\gamma_2^2 + k_{11})}{2k_{12} Z_d} \\ & - A_3 \frac{(Z_d - \gamma_1 Z_0)(\gamma_1^2 + k_{11})}{2k_{12} Z_d} \\ & - A_4 \frac{(Z_d - \gamma_2 Z_0)(\gamma_2^2 + k_{11})}{2k_{12} Z_d} \end{aligned} \tag{23}$$

or

$$V_3^- \doteq qA_1 + rA_2 + sA_3 + tA_4 \tag{24}$$

and,

$$V_3^+ = sA_1 + tA_2 + qA_3 + rA_4 \tag{25}$$

The procedures are similar for ports 2 and 4; the only difference is that, for these two ports, the $e^{\gamma x}$ term corresponds to the incident wave and the $e^{-\gamma x}$ term corresponds to the refected wave.

$$[V^-] = [X]\,[A] \tag{26}$$

$$[V^+] = [Y]\,[A] \tag{27}$$

where $[X]$ and $[Y]$ are matrices of the constants, m, n, o etc. and $[A]$ is a vector of A_i's. From (26) and (27), we have,

$$[V^-] = [X]\,[Y]^{-1}\,[V^+] \tag{28}$$

$$S_{11} = \left[\frac{o(mr - nq)e^{(\gamma_1+\gamma_2)w} + m(sn - or)e^{(\gamma_2-\gamma_1)w} + n(oq - ms)}{m(mr - nq)e^{(\gamma_1+\gamma_2)w} + o(sn - or)e^{(\gamma_2=\gamma_1)w} + p(oq - ms)}\right] \tag{30a}$$

$$S_{12} = \left[\frac{r(m^2 - 0^2)e^{\gamma_2 w} + q(op - mn)e^{\gamma_1 w} + s(on - mp)e^{-\gamma_1 w}}{m(mr - nq)e^{(\gamma_1+\gamma_2)w} + o(sn - or)e^{(\gamma_2-\gamma_1)w} + p(oq - ms)}\right] \tag{30b}$$

$$S_{14} = \left[\frac{n(m^2 - 0^2)e^{\gamma_2 w} + w(op - mn)e^{\gamma_1 w} + o(on - mp)e^{-\gamma_1 w}}{m(mr - nq)e^{(\gamma_1+\gamma_2)w} + o(sn - or)e^{(\gamma_2-\gamma_1)w} + p(oq - ms)}\right] \tag{30c}$$

$$S_{32} = \left[\frac{r(q^2 - s^2)e^{\gamma_2 w} + q(st - rq)e^{\gamma_1 w} + s(sr - qt)e^{-\gamma_1 w}}{q(mr - nq)e^{(\gamma_1+\gamma_2)w} + s(sn - or)e^{(\gamma_2-\gamma_1)w} + t(oq - ms)}\right] \tag{30d}$$

$$S_{34} = \left[\frac{n(q^2 - s^2)e^{\gamma_2 w} + m(st - rq)e^{\gamma_1 w} + o(sr - qt)e^{-\gamma_1 w}}{q(mr - nq)e^{(\gamma_1+\gamma_2)w} + s(sn - or)e^{(\gamma_2-\gamma_1)w} + t(oq - ms)}\right] \tag{30e}$$

$$S_{33} = \left[\frac{s(mr - nq)e^{(\gamma_1+\gamma_2)w} + q(sn - or)e^{(\gamma_2-\gamma_1)w} + r(oq - ms)}{q(mr - nq)e^{(\gamma_1+\gamma_1)w} + s(sn - or)e^{(\gamma_2-\gamma_2)w} + t(oq - ms)}\right] \tag{30f}$$

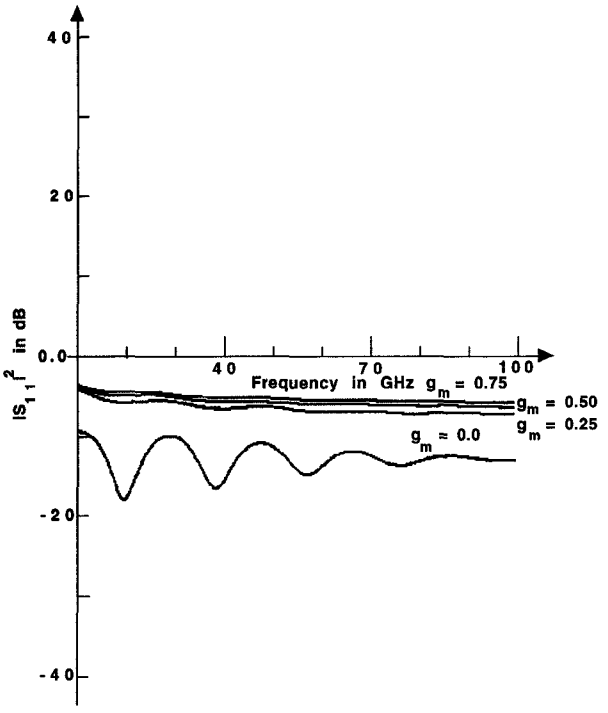

Fig. 5. A plot of $|S_{11}|^2$ as a function of frequency. Values of g_m are in S per mm and width w is 1 mm.

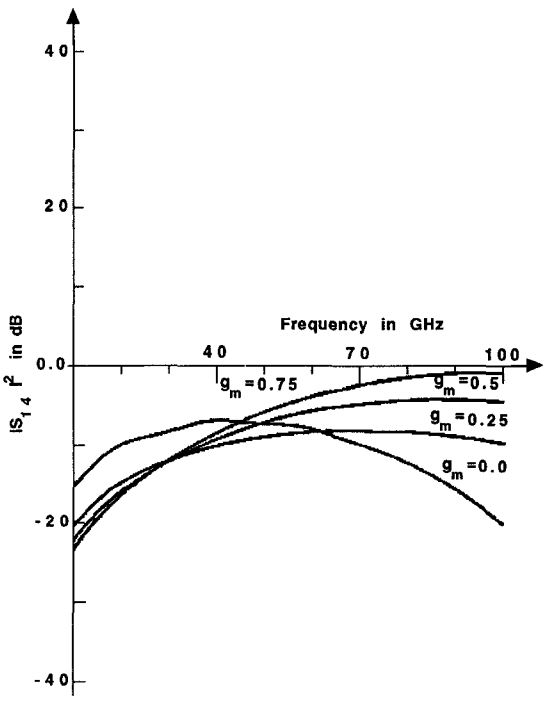

Fig. 6. A plot of $|S_{14}|^2$ as a function of frequency. Values of g_m are in S/mm and width w is 1 mm.

The S-matrix is therefore,

$$[S] = [X][Y]^{-1} \tag{29}$$

After carrying out the algebra involved, we obtain the closed form expressions for the S-parameters, shown in (30a)–(30f) at the bottom of the previous page where, "w " is the width of the device.

If the normalization impedances are desired to be unequal at the different ports, the above S-matrix can be transformed to account for that fact. Such transformation is described elsewhere [9].

Figs. 5–8 show the variation of the different S-parameters as a function of frequency and for different values of g_m. For these plots the characteristic impedance of the feeder transmission lines is assumed to be 50 ohms; further in order to demonstrate the existence of growing waves in the device the following equivalent circuit parameters were selected:

$G_{ds} = 1 \times 10^{-4}$ S/mm (the channel is assumed to be in the pinched-off condition)

$G_1 = 1 \times 10^{-3}$ S/mm and

$C_1 = 0.048467$ pF/mm.

As shown in Fig. 5 the magnitude of S_{11} fluctuates with frequency, the variations becoming less with increasing g_m. We believe this behavior is due to "Fabry–Perot" resonances caused by mismatches at the boundaries between the device and the feeder transmission lines. Similar resonances are also apparent in the behavior of the drain reflection coefficient S_{44} (Fig. 8).

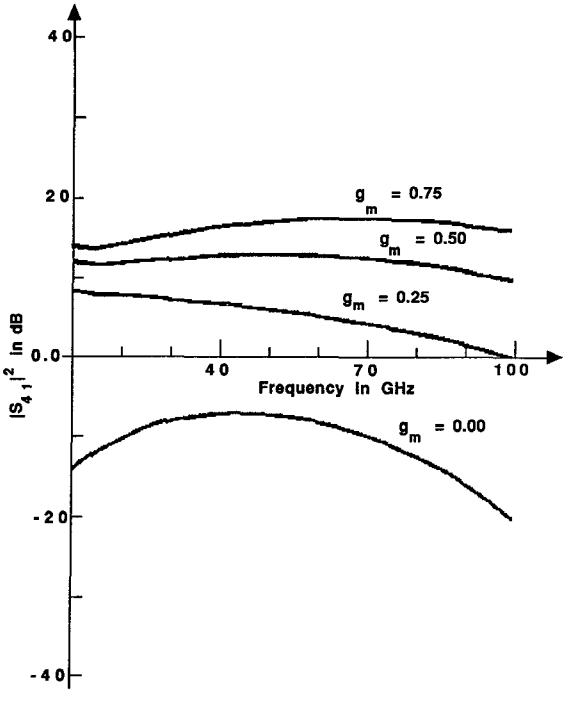

Fig. 7. A plot of $|S_{41}|^2$ as a function of frequency. Values of g_m are in S/mm and width w is 1 mm.

In general, the isolation between the gate and drain decreases with increasing frequency. This behavior is depicted in Fig. 6. The behavior of the power gain of the device is shown in Fig. 7. The desired flat frequency response of the gain is seen to be present over the frequency range considered; the gain does not fall off rapidly with increasing frequency and the power gain of the device exceeds 10 dB over the whole frequency range, 10 GHz to 100 GHz, for $g_m = 0.5$ S/mm.

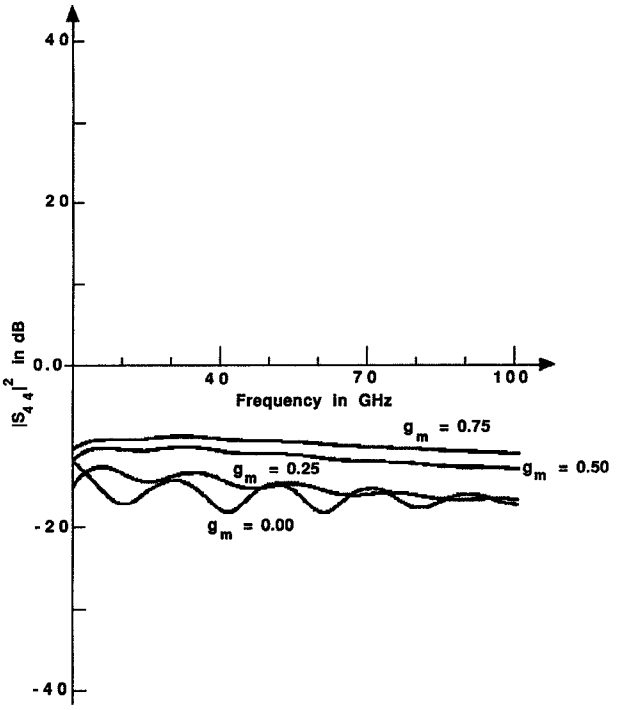

Fig. 8. A plot of $|S_{44}|^2$ as a function of frequency. Values of g_m are in S/mm and width w is 1 mm.

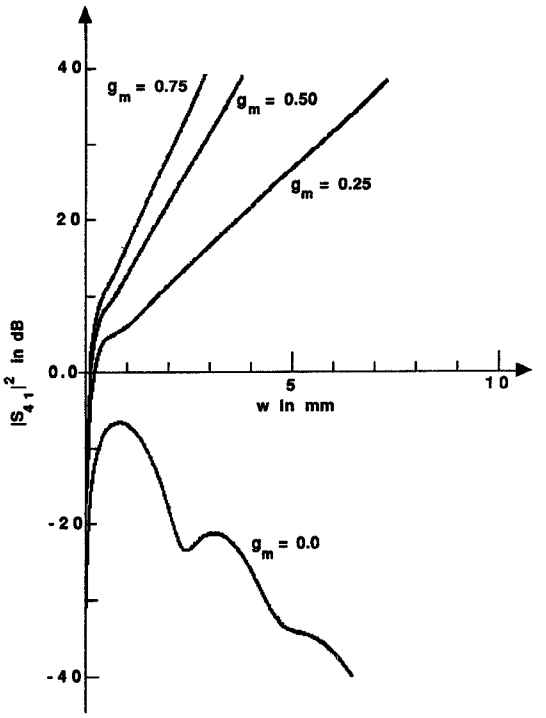

Fig. 9. A plot of $|S_{41}|^2$ as a function of device width at 50 GHz. Values of g_m are in S/mm.

Fig. 9, showing the power gain as a function of the device width, clearly illustrates the definite presence of a growing mode in the device; $|S_{41}|^2$ increases exponentially with device width, with the power gain exceeding 20 dB at 50 GHz for $w = 2$ mm and $g_m = 0.5$ S/mm. A signal growth rate of more than 10 dB/mm is indicated at 50 GHz for $g_m = 0.5/\text{mm}$. Further, the growth rate increases with increasing g_m.

IV. Summary

We have proposed a traveling-wave high electron mobility transistor. Such a device is expected to combine the inherently higher gain of HEMT's with traveling-wave action to provide high gain, high bandwidth performance at millimeter wave frequencies.

The proposed device is unique in that it includes an integral distributed load resistor and load capacitor. A rigorous analysis of the device has been carried out based on a transmission line model. Dispersion relations have been derived for the modes present in the device. It has been shown that the presence of a growing mode in the device is dependent on the equivalent circuit parameter values. In this context, usefulness of the integral load resistor and load capacitor as relatively easily controlled design parameters, prior to fabrication of the device, has been demonstrated.

Closed form expressions have been derived for the S-parameters of the device, we believe for the first time using device parameters value from published literature.

For a device width of 1 mm and transconductance of 0.5 S/mm, the theoretical power gain has been shown to be in excess of 10 dB for the whole range of frequencies from 10 GHz to 100 GHz. A remarkably flat theoretical frequency response has also been demonstrated, with the gain varying by not more than 2 dB over the entire frequency range, from 10 GHz to 100 GHz. Thus, although more work needs to be done in characterizing the device, in terms of noise performance and stability, the proposed THEMT seems to be a promising candidate for high gain amplification in the millimeter wave frequency range.

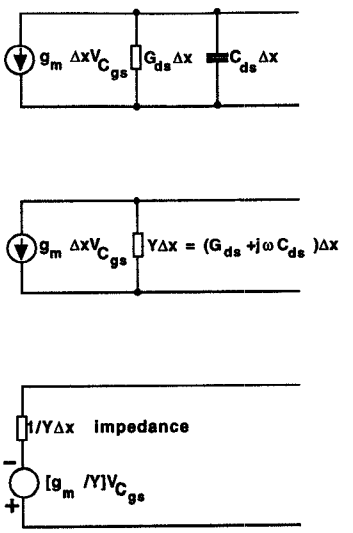

Fig. 10. Reduction of current source and parallel elements to voltage source and a series element.

Appendix

Derivation of Admittance Parameters M_{ij}

Referring to Fig. 2, we notice that the combination of the current source g_m, and the components C_{ds} and G_{ds} in parallel

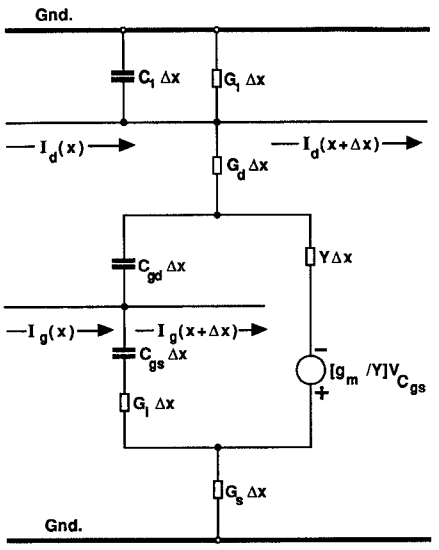

Fig. 11. Circuit used for deriving admittance parameters M_{ij}.

to it, can be reduced to a voltage source and a series element. The reduction is shown in Fig. 10. Referring to Fig. 11, which is just a part of the complete equivalent circuit, we can write the following nodal equations:

$$[I_g(x+\Delta x) - I_g(x)]/\Delta x = I_1/\Delta x - I_2/\Delta x \quad \text{(A1)}$$

$$[I_d(x+\Delta x) - I_d(x)]/\Delta x = -I_1/\Delta x - I_3/\Delta x - (G_1 + j\omega C_1)V_d(x+\Delta x) \quad \text{(A2)}$$

The aim is to eliminate I_1 and I_2 in the above equations, in terms of $V_g(x+\Delta x)$ and $V_d(x+\Delta x)$. Let us define:

$$I_A = I_1 + I_3 \quad \text{(A3)}$$

$$I_B = I_2 - I_1 \quad \text{(A4)}$$

This, it is required to obtain I_A and I_B in terms of $V_g(x+\Delta x)$ and $V_d(x+\Delta x)$. Referring again to Fig. 11, we can write the following loop equations:

$$V_g(x+\Delta x) = [1/j\omega C_{gs} + 1/G_i + 1/G_s] \cdot I_2/\Delta x + [1/G_s]I_3/\Delta x \quad \text{(A5)}$$

$$V_d(x+\Delta x) = [1/G_d + 1/Y + 1/G_s] \cdot I_3/\Delta x + [1/G_D]I_1/\Delta x + [1/G_s - g_m/j\omega C_{gs}Y]I_2/\Delta x \quad \text{(A6)}$$

$$0 = [1/j\omega C_{gd}]I_1/\Delta x + [1/j\omega C_{gs} + 1/G_i + g_m/J\omega C_{gs}Y]I_2/\Delta x - [1/Y]I_3/\Delta x \quad \text{(A7)}$$

Substituting the defining (A3) and (A4) into the above three equations, we obtain:

$$V_g(x+\Delta x) = [1/G_s]I_A/\Delta x + [1/j\omega C_{gs} + 1/G_s + 1/G_i]I_B/\Delta x + [1/j\omega C_{gs} + 1/G_i]I_1/\Delta x \quad \text{(A8)}$$

$$V_d(x+\Delta x) = [1/G_D + 1/Y + 1/G_s]I_A/\Delta x + [1/G_s - gm/j\omega C_{gs}Y]I_B/\Delta x - [1/Y + g_m/j\omega C_{gs}Y]I_1/\Delta x \quad \text{(A9)}$$

$$0 = -[1/Y]I_A/\Delta x + [1/j\omega C_{gs} + g_m/j\omega C_{gs}Y + 1/G_i]I_B/\Delta x \cdot [1/j\omega C_{gd} + 1/j\omega C_{gs} + g_m/j\omega C_{gs}Y + 1/G_i + 1/Y]I_1/\Delta x \quad \text{(A10)}$$

Using (A10), I_1 can be eliminated from (A8) and (A9) to obtain the following expressions:

$$V_G(x+\Delta x) = N_{11}I_A/\Delta X + N_{12}I_B/\Delta x \quad \text{(A11)}$$

$$V_D(x+\Delta x) = N_{21}I_A/\Delta X + N_{22}I_B/\Delta x \quad \text{(A12)}$$

Inverting the above N-matrix, we can obtain expressions for $I_A/\Delta x$ and $I_B/\Delta x$ in terms of $V_g(x+\Delta x)$ and $V_d(x+\Delta x)$. Substituting these results into (A1) and (A2) then, gives us the required M -parameters.

REFERENCES

[1] G. McIver, "A traveling-wave transistor," *Proc. IEEE,* vol. 53, pp. 1797–1798, 1965.
[2] W. Jutzi, "Uniform distributed amplifier analysis with fast and slow waves," *Proc IEEE,* vol. 56, pp.66–67, 1968.
[3] G. Kohn and R. Landauer, "Distributed field-effect amplifiers," *Proc. IEEE,* vol. 56, pp. 1136–1137, 1968.
[4] A. S. Podgorski and L. Y. Wei, "Theory of traveling-wave transistors," *IEEE Trans. Electron Devices,* vol. ED-29, pp. 1845–1853, 1982.
[5] C.-J. Wei, "Novel design of traveling-wave FET," *Electron Lett*, vol. 19, pp. 461–463, 1983.
[6] A. J. Holden, D. R. Daniel, I. Davies, C. H. Oxley, and H. D. Rees, "Gallium arsenide traveling-wave field effect transistors," *IEEE Trans Electron Devices,* vol. ED-32, pp. 61–66, 1985.
[7] T. Henderson, M. I. Aksun, C. K. Peng, H. Morkoc, P. C. Chao, P. M. Smith, K. H. G. Duh, and L. F. Lester, "Microwave performance of a quarter micrometer gate low-noise pseudomorphic InGaAs/AlGaAs modulation-doped field effect transistor," *IEEE Electron Device Lett.,* vol. EDL-7, no. 12, pp. 649–651, 1986.
[8] J. D. Ryder, *Networks, Lines and Fields* Englewood Cliffs, NJ: Prentice-Hall, 1973.
[9] G. E. Bodway, "Circuit design and characterization of transistors by means of three-port scattering parameters," *Microwave J.,* vol. 11, no. 5, pp. 7-1–7-11, 1968.

M. B. Anand, photograph and biography not available at the time of publication.

Prasanta K. Ghosh (S'79–M'81–SM'91) received the Ph.D. in solid state science from Pennsylvania State University. His primary research interests include thin film growth and processes, nonlinear dielectric and optical materials and thin films, high speed electronic devices, surface acoustic wave devices. He is the co-inventor of a patent entitled, "Multi-Layer Circuit Structure with Thin Semiconductor Channels".

Dr. Ghosh is currently Associate Professor of Electrical and Computer Engineering Department at Syracuse University.

Philipp Kornreich (S'64–M'72) earned the B.S. in electrical engineering in 1962 from the Carnegie Institute of Technology in Pittsburgh, PA (now Carnegie Melon University). He was awarded the Ph.D. degree in electrical engineering in 1967 with a minor in solid state physics from the University of Pennsylvania in Philadelphia, PA.

He is currently a Full Professor in the Department of Electrical and Computer Engineering of Syracuse University. He served as Krantzberg Visiting Professor in 1981 at the Department of Electrical Engineering at the Technion (Israel Institute of Technology) in Haifa, Israel. He has been associated with the Photonics Center of Rome Laboratories Griffiss AFB Rome, NY since it was founded in 1988. Dr. Kornreich was employed as Senior Research Engineer for Sperry-Rand Univac in the Physics and Materials Research Group in Blue Bell, PA from 1958–1966. He was an Engineer in the Missile and Surface Radar Division of RCA in Moorestown, NJ from 1955–1958. His current research interests include electro-optic device technology and optical communications. His past research has included high speed electronic and tunneling devices, electro-optic imaging devices, and circuit design.

He is a Member of the Electron Devices Group of IEEE, APS, SPIE, Society of Sigma Xi, AAAS, AAUP. He has 25 Patents.

D. J. Nicholson, photograph and biography not available at the time of publication.